ChemComm

COMMUNICATION

View Article Online
View Journal | View Issue

Cite this: *Chem. Commun.*, 2025, **61**, 19929

Received 21st July 2025,
Accepted 6th November 2025

DOI: 10.1039/d5cc04105h

rsc.li/chemcomm

Ligand-responsive ON–OFF anion transport using copper-caged acylhydrazone transporters

Umesh Shivpuje, Manzoor Ahmad, † Naveen J. Roy and Pinaki Talukdar *

Reversibly gated stimuli-responsive anion transport utilizing acylhydrazone-based transporters is reported. Acylhydrazone-copper complexation makes hydrazone protons unavailable for binding and transport, whilst decomplexation using Na_2EDTA activates the ion transport.

Ion transport across bilayer membranes, facilitated by ion channels, carriers, and ion pumps, is vital for biological functions.[1] Malfunctioning of these systems could result in severe diseases like cystic fibrosis (channelopathies).[2,3] Artificial ion transport systems in the form of ion channels and ion carriers have emerged as an important class of compounds that promise therapeutic applications for treating channelopathies.[4] Moreover, chloride transport by these systems is known to induce chloride-mediated apoptosis to the cancer cells, opening up a new avenue to combat cancer.[5] However, controlled spatiotemporal activation is vital for target-specific applications, as classical transporters are known to affect healthy cells as well. Stimulus-responsive ion transport systems controlled by external stimuli, such as light, ligands, voltage, pH, enzymes, and redox switching, are rare.[6] Examples include reversibly gated light-responsive systems based on azobenzene[7] and stilbene,[8] and irreversibly gated systems that provide effective ON–OFF control for ion transport. Responsive systems whose activity is controlled through the input of multiple stimuli remain rare. These provide better ON–OFF control compared to light-responsive ones, which exhibit background transport activity arising from incomplete photoconversion. Our lab has reported reversibly gated systems based on acylhydrazone[9] and phenylhydrazone[10] photoswitches. In 2020, a foldamer-based reversibly gated ion channel was reported with transmembrane ion transport controlled chemically using Cu(II) ion and EDTA.[11] However, the use of complex foldamer molecules presents a challenge for the practical application of the system.

Herein, we report a similar reversibly gated ion transporter utilizing copper(II) and Na_2EDTA as an external stimulus employing simpler acylhydrazone copper complexes. Acylhydrazone-based compounds are known to exhibit ion binding properties like heteroditopic ion pair binding. They also possess excellent ion transport properties. Acylhydrazone-based ligands, upon complexation with copper ion, are known to provide –N=C–O–Cu linkage[12] by removing hydrazone protons. We, therefore, envisaged that the complexation of carefully designed acylhydrazone-based ion transporters with copper would make hydrazone protons unavailable for anion binding and subsequent transport (Fig. 1). Decomplexation with Na_2EDTA, which would remove the copper ions, would render anion binding and transmembrane ion transport activity by providing free hydrazone protons. Reversible control would be achieved using Na_2EDTA and Cu(II) as an external stimulus. We chose isophthalic biscarboxamide hydrazone-based systems **1a–1d** as active transporters, as similar molecules were found to be efficient ion transporters in our previous study.[9] These transporters were expected to show an ion-pair transport because of an ion-pair binding in similar systems reported by Chmielewski and coworkers.[13] However, only anion transport was observed, probably because the cation bound to the transporter would be exposed to the hydrophobic domains of the lipid membrane. Meanwhile, **2a** was chosen as the pro-transporter. Incorporating different substituents to the amide moiety was expected to fine-tune the ion transport behavior of these systems by changing their lipophilicities.

The active transporters **1a–1d** were synthesized from monohydrolyzed ester **3**, prepared from the reported literature.[9] Subsequently, **3** was coupled with aromatic amines **4a–4d** using EDC·HCl/HOBt to yield the amide derivatives **5a–5d**. The reaction of **5a–5d** with hydrazine hydrate, followed by coupling with 2-piconaldehyde, furnished the active transporters **1a–1d** (Scheme 1). Further, compound **1b** was recrystallized from methanol. The single crystal structure data are provided in the SI (Fig. S23 and S24).

Department of Chemistry, Indian Institute of Science Education and Research Pune, Dr Homi Bhabha Road, Pashan, Pune 411008, Maharashtra, India.
E-mail: ptalukdar@iiserpune.ac.in
† Present address: Chemistry Research Laboratory, Mansfield Road, Oxford, OX1 3TA, UK.

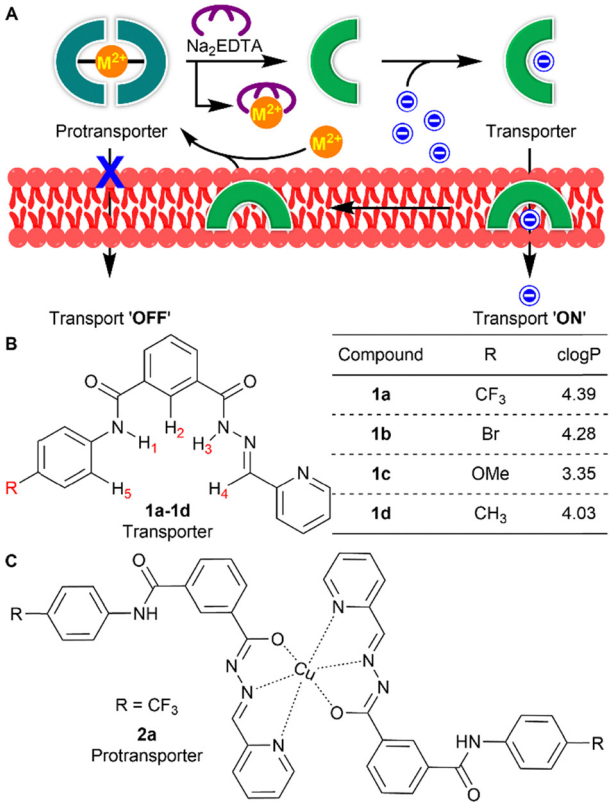

Compound	R	clogP
1a	CF_3	4.39
1b	Br	4.28
1c	OMe	3.35
1d	CH_3	4.03

Fig. 1 Working principle of ligand-responsive ion transport (A). Molecular structures of transporters **1a–1d** and their clogP values (B) and protransporter **2a**, respectively (C).

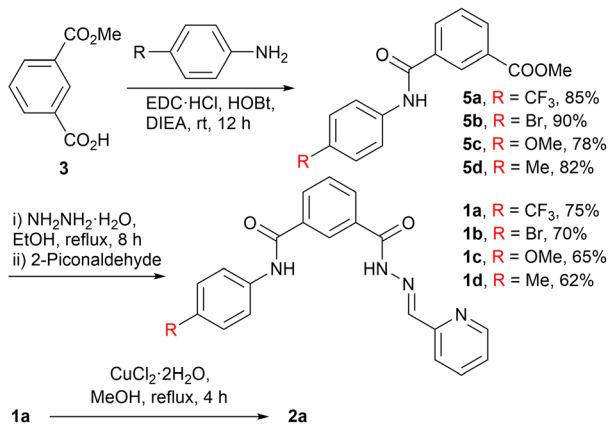

Scheme 1 Chemical synthesis of active transporters **1a–1d** and copper-caged protransporter **2a**.

Anion-binding affinities of **1a** were evaluated through ^{1}H NMR studies. Titration of **1a** with tetrabutylammonium chloride (TBACl), bromide (TBABr), iodide (TBAI) and nitrate ($TBANO_3$) salts in acetonitrile-d_3 led to significant downfield chemical shifts of the protons H_1, H_2, H_3, and H_4, indicating their involvement in anion binding through amide-$NH_1\cdots A^-$, ArC-$H_2\cdots A^-$, hydrazone-$NH_3\cdots A^-$, imine-$CH_4\cdots A^-$ hydrogen bonding interactions.

BindFit[14] analysis furnished a 1 : 1 (receptor: anion) binding stoichiometry with association constant values ($K_{a(1:1)}/Cl^-$) of $(9.1 \pm 0.7) \times 10^4$ M^{-1}, $K_{a(1:1)}/Br^-$ = $(3.47 \pm 0.1) \times 10^3$ M^{-1}, and $K_{a(1:1)}/I^-$ = 76.68 ± 4.9 M^{-1} and $K_{a(1:1)}/NO_3^-$ = 95.13 ± 0.41 M^{-1}, respectively (Fig. S3–S10). Further proof of chloride binding was obtained by high-resolution mass spectrometry (HRMS). Peaks at m/z = 447.0842 and 449.0818 corresponding to the [**1a** + Cl^-] complex were obtained in the solution state (Fig. S11).

The ion transport activity of the compounds **1a–1d** was evaluated across large unilamellar vesicles (LUVs).[5] 8-Hydroxy pyrene-1,3,6-trisulfonic acid trisodium salt (HPTS, 1 mM) was entrapped within the vesicles containing 100 mM of NaCl and 10 mM of HEPES buffer. A pH gradient (pH_{in} = 7.0 and pH_{out} = 7.8) was created across the lipid membrane by the addition of 0.5 M NaOH (20 μL) to the extravesicular solution. The subsequent addition of compounds **1a–1d** resulted in the collapse of the pH gradient, monitored by recording the change in fluorescence intensity at λ_{em} = 510 nm (λ_{ex} = 450 nm). The activity comparison yielded a transport activity sequence of **1a** > **1b** > **1c** > **1d** (Fig. 2A). Hill analysis of dose-dependent ion transport data furnished the EC_{50} values of 5.36 μM, 6.15 μM, and 46.31 μM for compounds **1a**, **1b**, and **1c**, respectively (Fig. S13 and S14). Hill coefficients (n) of ~1 indicated that ion transport across the lipid bilayer is mediated by a 1 : 1 receptor : anion interaction, and this result corroborates ^{1}H NMR titration studies. Hill analysis of **1d** could not be done due to its precipitation at higher concentrations.

Subsequently, Cl^- transport across EYPC–LUVs ⊃ lucigenin was monitored for the most active transporter **1a**. Vesicles entrapping lucigenin dye were prepared in a 200 mM $NaNO_3$ solution, and then a Cl^-/NO_3^- gradient was created by adding NaCl (33.3 μL, 2.0 M) in the extravesicular buffer. Chloride influx was evaluated by monitoring the change in the fluorescence intensity (λ_{ex} = 455 nm and λ_{em} = 535 nm) after the addition of **1a**. The dose-dependent Cl^- influx by **1a** is shown in Fig. S17. Hill analysis furnished an EC_{50} value of 9.34 μM with a Hill coefficient (n) of ~1 as obtained in the above-mentioned HPTS studies.

Mechanistically, ion transport in the lucigenin assay could occur through H^+/Cl^- symport, M^+/Cl^- symport, or Cl^-/OH^- antiport modes. However, varying anions in the external buffer using different NaX salts (X = Cl^-, Br^-, OAc^-, NO_3^-, and ClO_4^-) strongly affect the ion transport (Fig. 2B), and variation of extravesicular MCl salts (M = Li^+, Na^+, K^+, Rb^+, and Cs^+) in lucigenin-based studies did not change the ion transport (Fig. S19). These observations ruled out M^+/Cl^- symport and M^+/H^+ antiport, which indicated that ion transport could occur either through H^+/Cl^- symport or Cl^-/OH^- antiport mode. To get further insights, chloride efflux using **1a** was monitored using a chloride ion selective electrode (ISE) in the presence and absence of either valinomycin (a highly selective K^+ transporter) or monensin (an H^+/K^+ antiporter) with intravesicular KCl (300 mM) and extravesicular potassium gluconate (300 mM) solutions.[15] A significant enhancement in the Cl^- efflux rate was observed for **1a** in the presence of valinomycin, while it remained nearly unchanged with monensin. This enhanced Cl^- efflux in the presence of valinomycin provided evidence of transporter-mediated electrogenic transport. Selective K^+

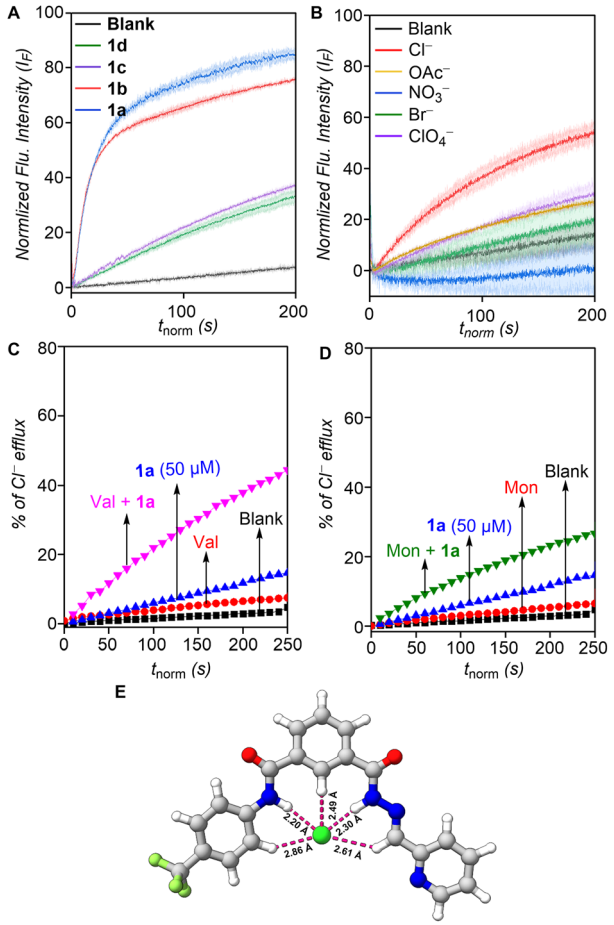

Fig. 2 Activity comparison of **1a–1d** (20.0 μM each) across EYPC–LUVs⊃HPTS (A). Anion selectivity of **1a** (3.5 μM) by varying external anions across EYPC–LUVs⊃HPTS (B). Normalized chloride efflux of **1a** in the presence and absence of valinomycin (C) and the presence and absence of monensin (D). The geometry-optimized structure of [**1a** + Cl^-] complex (E).

transport by valinomycin complements anion transport by **1a**, suggesting an antiport mechanism of transport (*i.e.*, Cl^-/OH^-). However, the lack of Cl^- efflux enhancement with monensin rules out an H^+/Cl^- symport mechanism for **1a** (Fig. 2C, D and Fig. S21).

The necessary evidence for a mobile carrier mechanism for ion transport was explored through experiments conducted in the liquid gel phase of dipalmitoylphosphatidylcholine (DPPC) large unilamellar vesicles (LUVs).[16] Inactivity at 25 °C, and restoration of activity at 45 °C, which is above the gel–liquid phase transition temperature for DPPC (T_m = 41 °C), is indicative of a mobile carrier process rather than transport mediated by self-assembly into an ion channel, that activity of which would be typically expected to be independent of the lipid phase (Fig. S18). Based on the experimentally determined Hill coefficient value of $n \sim 1$ the geometry-optimized structure of [**1a** + Cl^-] complex was obtained first by generating the most probable conformation by using the CONFLEX 8 program[17] (Fig. S25). Subsequently, the geometry optimization of the generated conformation was done by the Gaussian 09 program (see SI) using the B3LYP functional and 6-31G(d,p)[18] basis set. The geometry-optimized structure confirmed that the receptor participates in the anion recognition through amide-$NH_1\cdots Cl^-$ ($H\cdots Cl^-$ = 2.20 Å), hydrazone $NH_3\cdots Cl$ ($H\cdots Cl^-$ = 2.30 Å), imine $CH_4\cdots Cl^-$ ($H\cdots Cl^-$ = 2.61 Å), and Ar-$CH_5\cdots Cl^-$ ($H\cdots Cl^-$ = 2.86 Å) hydrogen bonding interactions (Fig. 2E and Fig. S27). The computed binding energy was found to be −45.02 kcal mol^{-1}.

The copper complexed protransporter **2a** was synthesized by refluxing the best active transporter **1a** with copper chloride dihydrate in methanol (Scheme 1). The broad peaks observed in the ^1H NMR spectra of compound **2a** indicate paramagnetic characteristics, which were further confirmed by EPR spectra, revealing the presence of an unpaired electron consistent with a $3d^9$ configuration (Fig. S2). The lack of acyl hydrazone-NH_3 proton in the ^1H NMR spectrum of **2a**, along with the (Cu^{2+}) $3d^9$ configuration confirmation through EPR, suggests the bonding structure of **2a** is –N=C–O–Cu. Furthermore, to assess the rigidity of [Cu(**1a**)$_2$], variable-temperature (VT) EPR measurements were conducted. The results showed no difference in the g value, indicating that [Cu(**1a**)$_2$] remains stable from 100 K to 300 K.11 The decomplexation of copper–hydrazone complex **2a** to form **1a** using Na_2EDTA was initially analyzed by ^1H NMR spectroscopy. Na_2EDTA solution in D_2O was added to a sample of **2a** in DMSO-d_6, and the NMR spectrum was recorded. ^1H NMR of the copper complex was observed to be broad due to the paramagnetic characteristics of the Cu-d^9 system. However, the addition of Na_2EDTA led to the appearance of NMR peaks, such as the hydrazine N–H_3 at 12.25 ppm and the Ar C–H_5 proton at 7.5 ppm. All these changes indicate the formation of active transporter **1a** (Fig. S22). The decomplexation of compound **2a** was additionally confirmed through UV-Vis absorption analyses. The absorbance observed at 370 nm for compound **2a** (20 μM) in MeOH : H_2O (9 : 1) solvent may be due to a charge transfer (CT) transition.[19] The stepwise addition of Na_2EDTA to **2a** led to a hypochromic shift at 370 nm and a hyperchromic shift seen at 297 nm, indicative of the formation of **1a** from **2a** which was validated by the absorbance measurement of compound **1a** in the same solvent at a concentration of 37 μM (Fig. 3A). Approximately 1.4 equivalents of Na_2EDTA were required to fully decomplex compound **2a** during this titration. This analysis also revealed a rapid decoupling of the copper hydrazone complex upon addition of Na_2EDTA. The quick disappearance of the 370 nm peak associated with copper ligand interaction confirmed the efficacy of the ligand exchange process. After analyzing the decomplexation of **2a** in the solution phase, responsive ion transport studies were performed in HPTS-based vesicular experiments, as mentioned earlier. Compound **2a** at 10 μM concentration did not show any ion transport activity, while transporter **1a** at the same concentration displayed maximal activity. The significant improvement in fluorescent intensity after decomplexation of **2a** with Na_2EDTA, suggests the formation of **1a** (Fig. 3B). Additionally, reversible **ON–OFF** ion transport assay was conducted by utilizing Na_2EDTA and copper as external triggers (Fig. 3C). When Na_2EDTA (1.4 eq.) was added to the solution of **2a** (20 μM in DMSO) to chelate Cu(II), it resulted in a marked enhancement in ion transport, while the addition of copper chloride

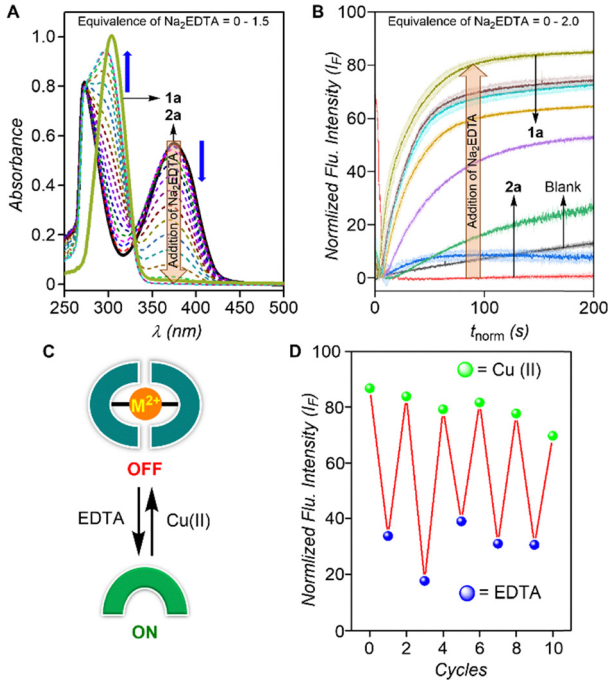

Fig. 3 UV titration of compound **2a** is represented with the addition of Na_2EDTA (A). Ion transport activity of **2a** (10 μM) upon addition of Na_2EDTA across EYPC–LUVs⊃HPTS (B). Schematic representation of OFF–ON responsive behavior (C). ON–OFF ion transport activity of **2a** upon addition of Na_2EDTA and Cu(II) ions (D).

dihydrate (1.1 eq.) to the activated solution halted the ion transport activity. This ON–OFF ion transport behavior using two distinct stimuli was successfully maintained across multiple cycles with minimal loss in performance (Fig. 3D).

In conclusion, we have developed reversibly-gated stimuli-responsive anion transporters based on acylhydrazones frameworks, exemplified by compound **1a**. Coordination of **1a** with Cu(II) ions affords a 2 : 1 stoichiometric complex **2a**, which remains inactive towards anion transport owing to the sequestration of the hydrazone proton essential for anion recognition. Subsequent decomplexation with Na_2EDTA restores the free hydrazone form **1a**, thereby reinstating its anion transport activity. Reversible ON–OFF switching of ion transport was reproducibly achieved over multiple cycles by the alternate addition of Cu(II) ions and Na_2EDTA as external chemical stimuli. This study highlights the utility of metal–ligand coordination as a dynamic regulatory element in the design of stimuli-responsive molecular systems capable of controlled chloride transport. The present strategy is anticipated to be transferable to congeners **1b–1d** and other appropriately designed ligands, providing a versatile platform for the development of bioinspired materials with potential therapeutic relevance.

PT acknowledges the financial support from the Anusandhan National Research Foundation (ANRF) (Project No. CRG/2022/001640) and the Indian Institute of Science Education and Research (IISER), Pune. US thanks the University Grants Commission (UGC), Govt of India, for a fellowship (UGC-NFOBC). MA thanks the University Grants Commission (UGC), Govt of India, for a fellowship. NR acknowledges the Council of Scientific and Industrial Research (CSIR), Govt of India, for a research fellowship.

Conflicts of interest

There are no conflicts to declare.

Data availability

All supporting data for this article are provided in the supplementary information (SI). Supplementary information is available. See DOI: **https://doi.org/10.1039/d5cc04105h**.

CCDC 2473653 (**1b**) contains the supplementary crystallographic data for this paper.[20]

Notes and references

1 T. J. Jentsch, C. A. Hübner and J. C. Fuhrmann, *Nat. Cell Biol.*, 2004, **6**, 1039–1047.
2 D. C. Gadsby, P. Vergani and L. Csanády, *Nature*, 2006, **440**, 477–483.
3 G. Bernard and M. I. Shevell, *Pediatr. Neurol.*, 2008, **38**, 73–85.
4 R. Planells-Cases and T. J. Jentsch, *Biochim. Biophys. Acta, Mol. Basis Dis.*, 2009, **1792**, 173–189.
5 T. Saha, M. S. Hossain, D. Saha, M. Lahiri and P. Talukdar, *J. Am. Chem. Soc.*, 2016, **138**, 7558–7567.
6 S. Chattopadhayay and P. Talukdar, *Curr. Opin. Chem. Biol.*, 2025, **85**, 102582.
7 W. Szymański, J. M. Beierle, H. A. V. Kistemaker, W. A. Velema and B. L. Feringa, *Chem. Rev.*, 2013, **113**, 6114–6178.
8 S. J. Wezenberg, L.-J. Chen, J. E. Bos, B. L. Feringa, E. N. W. Howe, X. Wu, M. A. Siegler and P. A. Gale, *J. Am. Chem. Soc.*, 2022, **144**, 331–338.
9 M. Ahmad, S. Chattopadhayay, D. Mondal, T. Vijayakanth and P. Talukdar, *Org. Lett.*, 2021, **23**, 7319–7324.
10 M. Ahmad, D. Mondal, N. J. Roy, T. Vijayakanth and P. Talukdar, *ChemPhotoChem*, 2022, **6**, e202200002.
11 A. D. Peters, S. Borsley, F. della Sala, D. F. Cairns-Gibson, M. Leonidou, J. Clayden, G. F. S. Whitehead, I. J. Vitórica-Yrezábal, E. Takano, J. Burthem, S. L. Cockroft and S. J. Webb, *Chem. Sci.*, 2020, **11**, 7023–7030.
12 S. Mondal, S. Naskar, A. K. Dey, E. Sinn, C. Eribal, S. R. Herron and S. K. Chattopadhyay, *Inorg. Chim. Acta*, 2013, **398**, 98–105.
13 Z. Kokan and M. J. Chmielewski, *J. Am. Chem. Soc.*, 2018, **140**, 16010–16014.
14 P. Thordarson, *Chem. Soc. Rev.*, 2011, **40**, 1305–1323.
15 L. Rose and A. T. A. Jenkins, *Bioelectrochemistry*, 2007, **70**, 387–393.
16 A. Kerckhoffs and M. J. Langton, *Chem. Sci.*, 2020, **11**, 6325–6331.
17 (*a*) H. Goto and E. Osawa, *J. Am. Chem. Soc.*, 1889, **111**, 8950–8951; (*b*) H. Goto, S. Obata, N. Nakayama and K. Ohta, *CONFLEX 8*, CONFLEX Corporation, Tokyo, Japan, 2017.
18 A. D. Becke, *J. Chem. Phys.*, 1993, **98**, 5648–5652.
19 A. K. Patel, R. N. Jadeja, H. Roy, R. N. Patel, S. K. Patel, R. J. Butcher, M. Cortijo and S. Herrero, *Polyhedron*, 2020, **186**, 114624.
20 CCDC 2473653: Experimental Crystal Structure Determination, 2022, DOI: **10.5517/ccdc.csd.cc2p1182**.

